Ground Support 2016 — A.A. Editor and B. Editor (eds)
ISBN 978-0-98709xx-x-x

Integrating microseismic and 3D stress monitoring with numerical modeling to improve ground hazard assessment

A. Tonnellier, C. Bouffier, V. Renaud, P. Bigarré, INERIS, France

S. Mozaffari, A. Nyström, P. Fjellström, BOLIDEN, Sweden

Abstract

INERIS and BOLIDEN are developing at Garpenberg mine (Sweden) new methodologies to monitor and to assess both quasi-static stress changes and ruptures in a seismic-prone area subject to deep mass-mining production. To achieve monitoring, a local mine seismic network has been deployed in the beginning of 2015 in the Lappberget area between 1100 and 1250 meter depth, in addition to 3D stress monitoring cells. Such network has been designed to fit with the sublevel stoping method and with the paste fill production/distribution system used by Boliden. Geophysical and geotechnical data are acquired continuously and near-to real time transferred to INERIS data centre through e.cenaris e.infrastructure for automated data processing and database management, along with mining datasets. In addition to continuous monitoring, a fine-grid 3D numerical model of the mine has been defined, in which the complex 3D shapes of the orebody and a major weakness unit are taken into account. It is submitted to successive step-by-step (exploited + backfilled stopes) simulations to assess the stress variations following a correct stress path, the plastic state, the safety factor, the strain and displacement fields, both elastic and plastic (shear and volumetric strain) energies in the mine in response to its development as stresses are monitored for quantitative comparison. Until November 2015, up to 20.000 m^3 of ore were extracted within the monitored area, highlighting numerous stress shifts ranging from 0.1 MPa to 15 MPa with the stress cells. Methodology and data presented here are the preliminary results of the first year of monitoring. The study focuses on 3 main stress shifts recorded by the stress cells at level 1157, which are associated with the recorded seismicity, and then compared to the numerical model. Indeed significant immediate and differed stress shifts associated with induced microseismic events are recorded over a several-week period following the first blasts. In addition, modeling reveals that the presence of weak horizon (talc) influences the dynamic response of the mine by inducing creep and plasticity phenomena, which would explain the results obtained by geotechnical measurements and microseismicity.

Keywords: microseismic monitoring, stress shift, modeling, risk assessment

1 Introduction

Nowadays, the underground mining industry has developed high-technology mass mining methods to optimize productivity at deep levels. Massive extraction induces high-level stress redistribution, which may generate seismic events around mining works (Gibowicz and Kijko 1994). Numerous authors have already highlighted the necessity of steadily enhanced scientific practices and technologies to face mining-induced seismicity and rockburst hazards, in order to guarantee the safety of both miners and the mining environment (Ortlepp 1997, Durrheim et al. 2006, Durrheim 2010, Hudyma and Potvin 2010). In this context, Hudyma and Potvin (2010) have proposed an engineering approach based on the application of microseismic monitoring to identify the active seismic sources, to assess the related risks, and to implement suitable mitigating measures. Most of these monitoring activities have been successfully applied in deep mines in Canada, South Africa, and Australia (Hudyma and Potvin 2010) where production depths easily reach 2000 m and much deeper in South Africa. Similar applications are also being employed in

European mines subject to deep-production stress shift (Lizurek et al. 2014, Szczerbowski et al. 2015 in Poland, Janiszewski 2014 in Finland).

Geotechnical monitoring is currently used in numerous mines through the use of extensometers, crackmeters, etc. Maleki 1990 presents an example of a stability evaluation of a coal mine based on modeling coupled with borehole pressure cells and deformation measurements. Studies realized by Potvin and Wesseloo (2013) present a well-documented example of instrumented mine in Tasmania with implementation of seismic network and CSIRO HI cells measurements, showing a strong correlation between the mining blasts, large seismic events and the stress changes measured by close instruments. Nevertheless, geotechnical sensors provide accurate information on aseismic deformations locally and depending on the mining method they may be costly to deploy.

Eventually, monitoring the mining process is essential to fulfill a geohazard assessment routine based on geotechnical and seismic methods. Indeed, huge-stress transfers and rock failures are generated by the mining process itself around the freshly created excavation. High-quality technological mine data is nowadays becoming full part of the near-to real-time mine data flow, promising some interesting breakthrough in the quantitative rockmass response. Furthermore, combining seismic and geotechnical data analysis together with a 3D mine-data-based numerical model shows potential to build a more complete understanding of the rockmass response. The aim is finally to improve geohazard management in mines.

The I2Mine (Innovative Technologies and Concepts for the Intelligent Deep Mine of the Future) FP7 European project has been developed to propose activities designed to realize the concept of an invisible, zero-impact mine and to enhance the development of technologies suitable for deep mining activities. In this context, INERIS (National Institute for Industrial Environment and Risks) in partnership with the Swedish mining company Boliden, are currently implementing a new global monitoring approach in a new deep orebody, consisting in coupling both microseismic and stress monitoring observations with 3D modeling, as a challenging data integration solution to complete the geomechanical overview of the local (stress) and global (microseismic) dynamic mine response to the production. In this paper, the Garpenberg mine (Sweden) is introduced as well as the monitoring system that has been deployed, including acquisition, transmission process and data fusion together with production and geological mine data. The analysis focuses on a 10 months dataset. An interpretation is proposed, based on the associated dynamic response (microseismicity) and correlated with the mine data (geology, production volumes) through modeling. Finally, additional more recent stress shifts are considered with the perspective to complete the analysis and to optimize the fusion of 3D stress, microseismic and mine production data together with 3D modeling stress prediction capabilities.

2 Study area

The Garpenberg mine is located in the Dalarna County and it is the oldest mine still in activity in Sweden. In this mine, ore is nowadays extracted using sublevel stoping with paste filling and long-hole drilling method. It produces about 2.5 million tons of ore per year, composed of zinc, silver, copper, lead and gold and has now reached production depths higher than 1300 m below surface. Stope production is optimized by dividing the whole ore in primary and secondary stopes. Producing primary stope might significantly increase the stress level in the secondary stopes, which may softly yield or not, inducing seismicity and provoke instabilities or even rockbursts. Proposing good stope production sequencing is hence essential to minimize high-stressed zones. Indeed, as reported by Larsson (2004), in November 2003 the Garpenberg mine experienced a high seismic activity associated to a rockburst at 835 m depth, an event that was perceived on the surface as if it was a production blast. This event was caused by a failure of the sill pillar and provoked spallings in the roof and walls to a depth of about 25 cm, displacing about 1 ton of rock (Nyström 2003). Richter magnitude was estimated between -1.0 and 0.0 from Hudyma & Potvin (2004) classification.

In response to this event, a microseismic monitoring network was installed in the upper levels of the Lappberget area (up to approximately 1100 m depth) by the Institute of Mine Seismology (IMS) (Froehlich, 2014). However, the current exploitation of the mine (Fig. 1) is reaching levels as deep as 1300 m for which the IMS network coverage is not appropriated. To this purpose, within the framework of the I2Mine project, it has been proposed to set up a new experimental stress and microseismic monitoring network in the deepest area of the mine, under INERIS supervision.

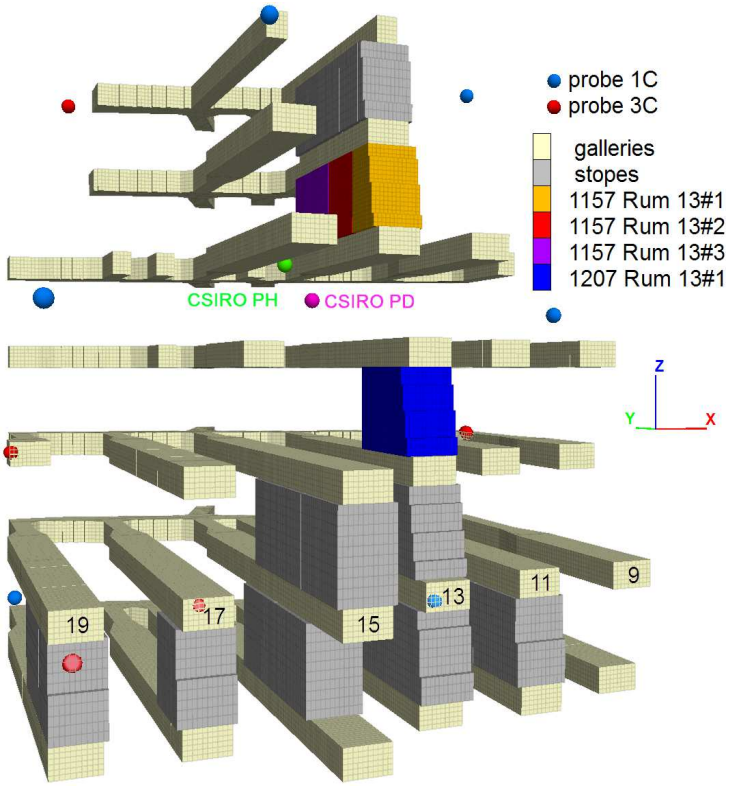

Figure 1 **3D view of Lappberget monitored section with successive stope production in yellow, red, purple and blue for the 4 stress shifts that are analyzed in the present study and in grey for the other productions. CSIRO cells and microseismic 1C and 3C probes are also indicated as well as the primary stopes number (from 9 to 19).**

3 Stress and microseismic monitoring

3.1 Monitoring network setup

Stress and microseismic sensors have been installed in a permanent way between December 2014 and February 2015 (Fig. 1). They were respectively pasted (with epoxy glue for CSIRO HI cells, well tested and documented in literature by Lahaie 2010) or grouted into horizontal, inclined, or vertical drilled holes. The location of these sensors was designed to guarantee significant stress changes in an area of interest considering the mine exploitation planning to come.

More specifically, the stress measurement layout consists of two stress cells installed at level 1157 (corresponding to the depth in meters) close to stope 13, planned to be mined in 2015-2016 (Fig. 1). PD CSIRO HI cell is set up in a downward borehole in stope 13 (primary stope) in the last section planned to be mined. In this way the monitoring network aims to assess the expected increase of the stress level in response to the progression of the nearby exploitation in a priori elastic conditions. PH CSIRO HI cell is set up in a horizontal hole in stope 14 (secondary stope) to compare the stress shifts between primary and secondary stopes until the end of the exploitation of the entire stope and maybe to reach the occurrence of failure. Each cell performs 12-strain measurements each hour with accuracy about ± 5µstrains, allowing

stress shift determination by inversion. These measurements provide very local but accurate information to be compared with 3D numerical models and help for their calibration.

This instrumentation was preceded by a stress measurement campaign with overcoring methods (Amadei and Stephansson 1997) using also CSIRO HI cells located in the same borehole as for PH permanent cell, in order to assess the initial stress state (i.e. before any mining activity) and the relevant elastic parameters of the rockmass. Indeed, this protocol allows to monitor the complete 3D stress path departing from the pre-existing stresses calculated in Table 1. The measurements obtained from overcoring are close each other in amplitude; however, a significant discrepancy, probably due to the stronger influence of the drift in H1, is observed. Global stress state from measurement is consequently calculated on the basis of H2 as a reference, less influenced by the drifts and closer to PH. Pre-existing stresses are also used as one of the most important input for model calibration.

Table 1 Measured pre-existing stress field calculated from the overcoring samples with azimuth and dip angles.

Measurement index	σ1(MPa) | Az.(°N) | Dip (°)	σ2(MPa) | Az.(°N) | Dip (°)	σ3(MPa) | Az.(°N) | Dip (°)
H1	54 | 40 | 9	38 | 310 | 2	25 | 210 | 81
H2	54 | 0 | 7	44 | 91 | 5	26 | 219 | 81

In addition, six 1-component (1C) and five 3-component (3C) microseismic probes, equipped with 14-Hz geophones, have been deployed over the area of interest extending from reference levels 1108 to 1257 with an average inter-distance of 150 m. Seismic signals are acquired following an automatic advanced triggering scheme with an 8 kHz-sampling frequency. Once detected, waveforms are transmitted through the Local Area Network for automatic association. The microseismic events are then located using an inversion-routine based on the Oct-Tree method (Lomax et al. 2000). It consists in identifying the best position of the seismic signals source over a meshed search grid, using P and S waves' arrival times and primary waves' polarization angles. Indeed, it has been proved that the localization of a seismic signal with few probes can be improved with the integration of the polarization angles (Magotra et al. 1987; Volker and Roth 2003). This approach has already been successfully applied in mine environments (Abdul-Wahed et al. 2001, Contrucci et al. 2010). Calculated P- and S-wave velocities have been estimated from five 0.5-to-2 Kg-load calibration blasts (V_P=6575 m s^{-1} and V_S=3703 m s^{-1}). They showed good agreement with the expected values for such geological context (Zinszner and Pellerin 2007; Pasquet 2014); and their ratio (V_P/V_S = 1.78) and the equivalent elastodynamic parameters (E = 70 GPa and v = 0.27) are coherent. In such set up context, location error can reach up to 25 m, or higher depending on the Signal-to-Noise Ratio respect to the high mine activity (Matrullo et al. 2015). Finally, the relationship to estimate the local magnitude M_L of these microseismic events is adjusted to fit IMS M_L estimates that focuses essentially on the Kasperboo mining area, approximately located over Lappberget area.

3.2 Data transfer

Data acquisition is ensured by three SYTGEM Acquisition Units (AU), situated at levels 1108, 1182 and 1257. The SYTGEM technology offers both geotechnical and microseismic monitoring capabilities, featuring smart protocols to couple the two types of monitoring: AUs are interconnected and linked to a supervising PC on surface, from which communication and data transfer to the processing laboratories are managed through a specialized remote processing and database infrastructure so-called e.cenaris. In the present study, both monitored data and mining production information (blasts location and time, produced volume and surrounding geology…) are collected and transferred, enabling to quickly and remotely access an overview of the rock mass response (stress, microseismic) versus mining activity.

4 Data analysis

4.1 Stress change measurements

In this study, three main strain shifts have been clearly measured between April and July 2015 through the stress cells at level 1157, plus an additional one in August 2015 at level 1207. These strain shifts were related to four important stope production blasts in the vicinity of the cells (up to 45 m between the excavation front and the cell location) as reported in Table 2. This table describes the main exploitation parameters, the distance of the excavated stope front to the CSIRO HI cells and the value of the most important stress change calculated after a given excavation (no indication of direction). The other stope excavations, considering their typical dimensions, were too far to be detected or with a very low signal so that inversion processing had no meaning.

Table 2 Details of the stope production blasts that were identified by the stress cells (positive value represent unloading).

Blast day (2015)	Depth (m)	Stope #Step	Load (kg) | volume (m^3)	Distance stope front - cells PH|PD (m)	Assessed max. stress shift Δσ PH|PD (MPa)
10/04/2015	1157	13#1	3553 | 1300	35 | 35	8.8 | 2.4
08/07/2015	1157	13#2	4212 | 2800	23 | 22	-1.0|-1.3
28/07/2015	1157	13#3	6669 | 6000	5 | 8	-14.0|-8.4
11/08/2015	1207	13#1	4172 | 2000	40 | 42	4.1|1.0

The strains recorded by the CSIRO HI cells after the blast (1157 13#1, 10/04/2015) present two features (Fig.2): firstly, the strain shift is unexpectedly important considering the mined volume (≈1300 m^3) and the distance between excavation front and CSIRO HI cells ≈35 m (note the difference between PD and PH measurements which is due to excavation geometry: PH cell is directly oriented toward the produced stope while PD cell is in a "grey area", as illustrated in Fig.1); secondly, additional strains are observed during several days after the blast (up to 1 month). The six-component stress shift tensor [Δσ] is assessed from the strains recorded by inversion calculation (Fig. 3 from PH measurements). The stress shift obtained immediately after the blast is much lower (5.6 MPa for the maximum amplitude) than the stress shift calculated on the basis of the cumulated strains until 10 days after the blast (8.8 MPa).

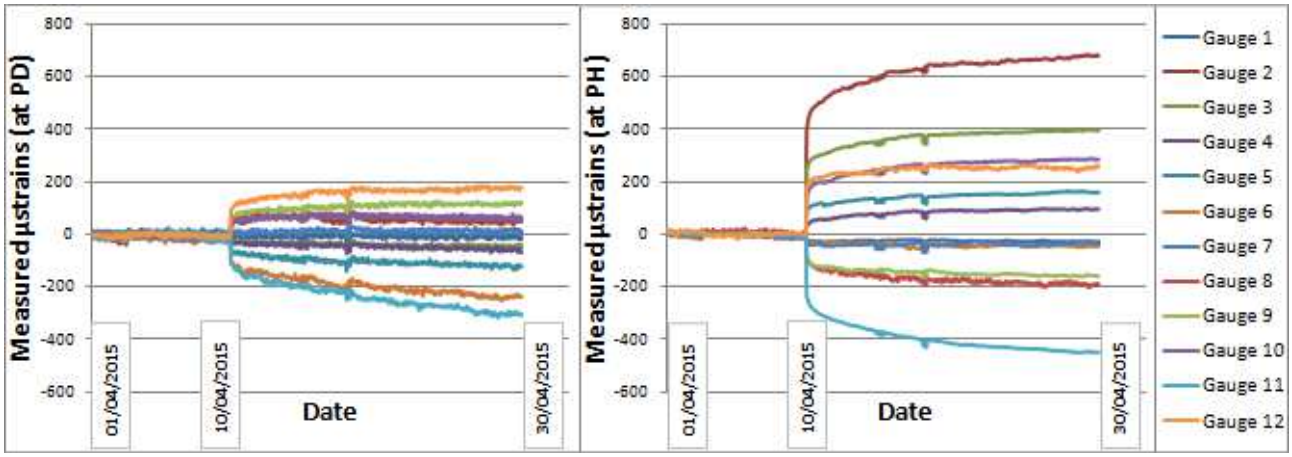

Figure 2 PD and PH strains recorded CSIRO HI cells (from 01/04/2015 to 30/04/2015).

On the contrary, the second blast performed at the same level (1157 13#2, 08/07/2015) is marked by a very low stress shift although the mined volume was much important (~2800 m^3) and the distance from the front of the excavation to the stress monitoring CSIRO HI cells was lower (~22 m). The third and last blast at this level (1157 13#3) completed the exploitation of the remaining volume of this trench. It corresponds to an important excavated volume (~6000 m^3) that was mined very close to the stress monitoring cells. The recorded strains are important with the emergence of plastic deformations at PH. In these conditions, the

hypothesis of an elastic model is not valid anymore, which as a consequence limits the accuracy for the assessment of successive stress shifts.

The additional strain shift recorded after blast 1207 13#1 corresponds to the beginning of the exploitation of stope 13 at a lower level. The strains recorded are also important compared to the mined volume and the distance of the front to the stress monitoring CSIRO HI cells, even if these features are less significant than for 1157 13#1 blast.

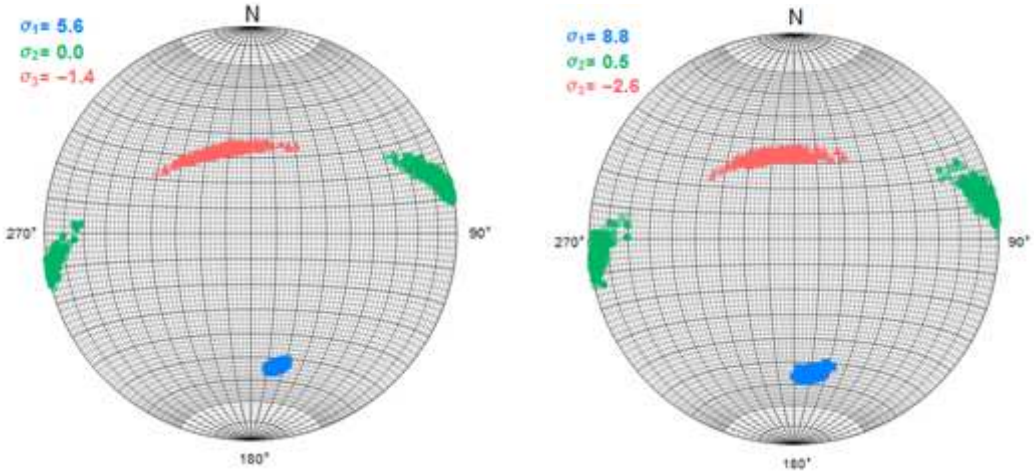

Figure 3 Stress shift assessments (in MPa) calculated with the strain shift recorded at the stress monitoring CSIRO HI cell PH after blast 1157 13#1 (10/04/2015). Left: shift between states immediately before and after the blast; right: shift between states immediately before the blast and 10 days after the blast. The indicated North corresponds to the predefined North of the mine (along Y axis on Fig. 1).

Such observations proved the responsiveness of the stress cells to the close mine production. To get a better understanding of the unexpected amplitudes of the 3D stress shifts, investigations are proposed further from microseismic data analysis and 3D modeling over the same areas and periods.

4.2 Microseismic activity

Quasi static stress monitoring yields information on the mining-induced stress field, wherever stress cells have been judiciously implemented to monitor the 3D stress path before any failure occurs. Seismic monitoring instead provides information about rocks at failure, i.e. wherever stresses have exceeded the rock strength locally. It has thus been proposed to analyze the microseismic events that were detected in the same periods and located in a radius of 25 m around each blast location (approximately 3-stope width) to identify possible correlations between the production, the stress shifts and the microseismic response. The cumulated number of microseismic events has hence been plotted per “post-blast period”, where a post-blast period starts the day of the blast and finishes one day before the next of the four blasts (Fig. 4). For the last blast, it has been arbitrarily decided to finish the period one month after the day of the blast (i.e. the 11/09/2015). The time interval between each selected blast is varying but the first objective of such illustration was to quantify possible cluster of microseismic events associated in the space and time domains with the production areas. Although the mining process appears geometrically quite repetitive from one step to another, the microseismic responsiveness to a mining blast is not regular: blasts of the 10/04/2015 and of the 28/07/2015 seem to be followed by local microseismic events during several days, while nearly no seismicity is observed after the blasts of the 08/07/2015 and of the 11/08/2015 or scarcely during the first day. Then, while most of the microseismic events after stope blasts of the 28/07/2015 are detected the same day and in higher quantity, it takes much longer for the blasts of the 10/04/2015. This approximately 1-week response corresponds to the stress stability-return period (Fig. 2), which could be considered as a time dependent de-stressing phase. Such period length might be associated with the local geology and ambient stress level before blasting. This is successively checked with modeling analysis.

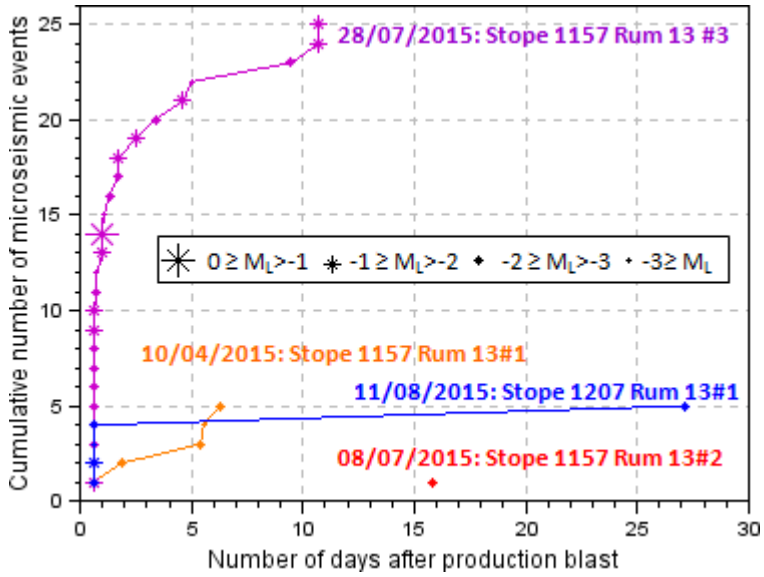

Figure 4 **Microseismic events detected and located in a 25 m-radius around each production blast over the corresponding post-blast periods. The size of the stars is proportional to the estimated M_L of the events, varying between -3 and 0. The plot colors correspond to the colors of the stopes as identified in Fig. 1.**

5 Modeling

3D numerical modeling remains the only practical mean to assess the total stress field features related to mining sequences and stability issues. It calls for cautiousness due to the inherent limitations of the technology, for which a very simplified description of the rock mass is considered compared to its real complexity (void geometries and contrasted geology). Moreover, the dimensions of the incremental mining steps are small compared to the mining area to be modeled. This requires the meshing to be fine enough to ensure a good calibration of the mining-induced stress field. Here both stress and seismic field monitoring becomes prominent to assess how relevant the computed stress field is and to recall how much a good knowledge of the pre-existing principal stresses is crucial to compute correct solutions of the mining-induced stress field at any stage of the mine development.

3D numerical modeling therefore starts with the determination of the initial stress field, before any mining activity at all. To this purpose, it is necessary to model all excavations phases that were carried out before the CSIRO cells were installed. A 3D numerical model is designed with Flac3D software (Itasca 2012), in which initial stresses are adjusted to make the computed induced stresses compatible with the pre-existing ones measured by the CSIRO cells, i.e. in a zone already influenced by previous mining overlying levels. This knowledge is all the more important, since all the common parameters (stresses, safety factor, plasticity, stored elastic energy, strains) will derive from the initial stress conditions.

The model must extend from the surface up to a sufficient depth for the model boundaries not to introduce significant artifacts. Concerning horizontal extensions, to limit the model size, the influence zone of the stress measurement is assumed to be over maximum 3 stopes on each side. Finally, the resulting 3D model has a volume of 2.7 km^3 over a 1500 m height and is composed of 10 600 000 hexahedral zones. One of the difficulties in this modeling is to deal with the simplified description of the ore body and weaknesses zones (mainly composed of talc that locally influences the stress field, composed of sericitic schist (soft) to talcy schist (very soft)). The chosen rheology for these materials is an elastoplastic law with a parabolic failure criterion (Hoek & Brown, 1997) and the geomechanical parameters needed in the model are determined from lab testing (Table 3).

Table 3 Geomechanical parameters retained for 3D modeling.

Parameter	Symbol	Unit	Ore	Limestone	Weakness body	Backfill
Density (mean of 3 tests)	ρ	[kg.m^{-3}]	3030	3030	3030	2000
Young's modulus	E	[GPa]	66	57	20	0.5
Poisson ratio	v	[-]	0.2	0.18	0.3	0.2
Comp. strength intact rock	σ_{ci}	[MPa]	188	110	30	-
Hoek & Brown parameters	m	[-]	10	10	1	-
	s	[-]	0.112	0.112	0.001	-

5.1 Initial stress determination

The stress calibration is processed by assuming test values in the model for the 3 principal initial stresses before any excavation happened; then the upper mining levels (from 578 m to 1088 m depth) are excavated and backfilled; and finally, the few recent drifts and the stopes excavated in the zone of influence of the field measurements before December 2014 are deleted in the model. In the present study, 2x3 initial stresses, which correspond to 2x6 total induced stresses (σ_{xx},σ_{yy},σ_{zz},σ_{xy},σ_{xz},σ_{yz}) have been computed at two different locations (H1 and H2, close to PH permanent cell, Fig. 1). When those computations are repeated sufficiently (computed stress data bank), it is possible to back-compute the stress states in those 2 locations that minimize the difference between measured and computed stresses. The minimization (Levenberg-Marquardt method, Levenberg 1944) is done on the following 3 *f* and 6 *g* order 2 polynomial functions (f_i & g_i): $\sigma_{xx}^{ini}=f_x(\sigma^{induced})$, $\sigma_{yy}^{ini}=f_y(\sigma^{induced})$, $\sigma_{zz}^{ini}=f_z(\sigma^{induced})$ and $\sigma_i^{induced}=g_i(\sigma_{xx}^{ini}$, σ_{yy}^{ini},σ_{zz}^{ini}) (i: 1 to 6). At the end, the best solution for both locations is determined when the domain of initial stresses is compatible with the confidence interval of measured stresses and densities (intersection of regions created with fitting functions g_i):

$$\sigma_i^{min}<g_i(\sigma_{xx}^{ini}, \sigma_{yy}^{ini},\sigma_{zz}^{ini}) < \sigma_i^{max} \text{ (i: 1 to 6)}$$
$$\rho_{min}.g.h<\sigma_{zz}^{ini}<\rho_{max}.g.h$$

For Lappberget section at -1155 m level, the retained computed initial stress state is:

σ_{xx}^{ini}= 44.3 MPa, σ_{yy}^{ini}= 47.3 MPa and σ_{zz}^{ini}= 3030 kg/m^3*g*1155 m = 34.3 MPa.

With these initial values, the maximal difference between the theoretical stress values and the values extracted from overcoring (Table 1) is of 2.5 MPa.

5.2 Field stress monitoring

The CSIRO cells permanently installed in locations PH and PD (Fig. 1) record stress shifts due to any significant excavation not far away. Theoretically, an excavation induces a stress shift proportional to the excavated volume and inversely proportional to the third power of the distance. To compare predicted stresses from numerical modeling to the measurements obtained with the permanent cells, a 12-stage phasing (gallery and stope excavations) has been carried out with the Flac3D model. At each stage, the stress components of the previous stage are subtracted to those of the current stage, exactly as stresses are measured by CSIRO cells. For the three strain shifts at level 1157, the comparison between modeled and measured stress shift (for the 3 principal stresses) can be analyzed from Fig. 5 and 6. A significant difference is noted for the excavation of 10/04/2015 (blast of 3553 Kg explosive for an approximate volume of 1300 m^3 of ore): maximum measured stress shift is 1.8 times greater than the maximum modeled stress shift. This is due to the presence of the weakness body: its geometry is evaluated by mine's geologist and then simplified in the model, which can lead to significant differences with the reality. Indeed, without taking the weakness body into account, the measured stress shift is 3 times lower than the modeled one. This proves the strong influence of much contrasted units neighboring the mining voids, inducing much higher stress transfer on the hardest rocks. On 28/07/2015, a bigger (2800 m^3) closer (22 m far from the cells) excavation occurred, which produced a lower stress shift than the excavation of 10/04/2015 (1300 m^3

at 35 m) according to the 3D model. This observation confirms the assumption that the presence of a weakness body (expected to be talc) may strongly impact the stress field. For both excavations, the cells located at both PH and PD measured the same trend as modeling: all principal stresses have the same sign (- for loading or + for unloading). Moreover, the analysis of the closer excavation (28/07/2015) shows that the modeled and measured stress shifts have different amplitudes for 2 components. The numerical model obviously overestimates the major principal stress and thus the stored strain energy. This can be explained by at least two reasons: 1) the CSIRO cells are in a damaged zone where stresses are not stabilized yet; 2) the simplified geometry of the real excavated stope is not accurate enough, as well as the influence of the surrounding geological discontinuities. One can suspect that modeling the paste-filling could reduce these differences.

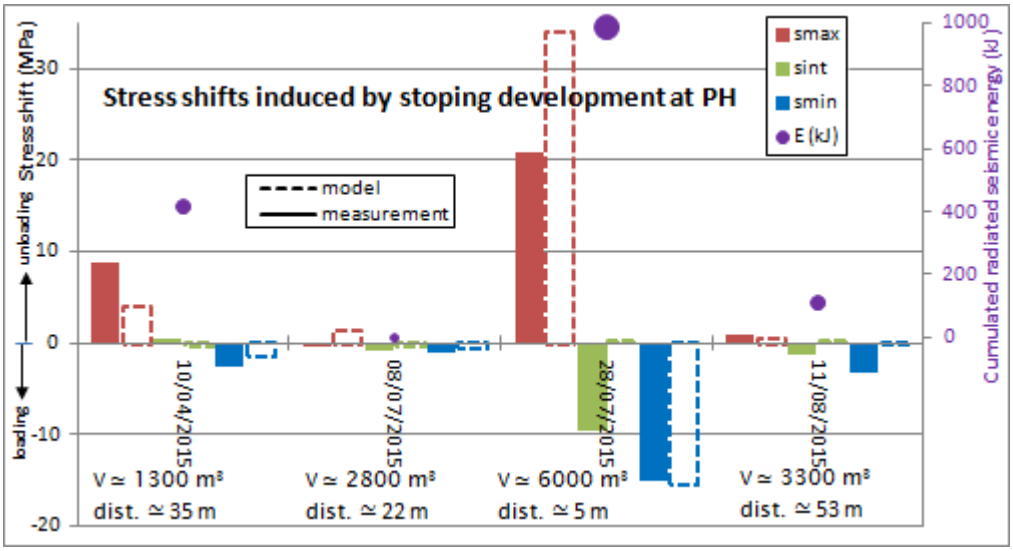

Figure 5 **Measured and modeled stress shifts (smax = major, sint = intermediate, smin = minor) induced by stoping development at PH between April and August 2015. Information on the excavated volume (V), the distance from the cells (dist.) and the cumulated radiated seismic energy (purple circle) are added.**

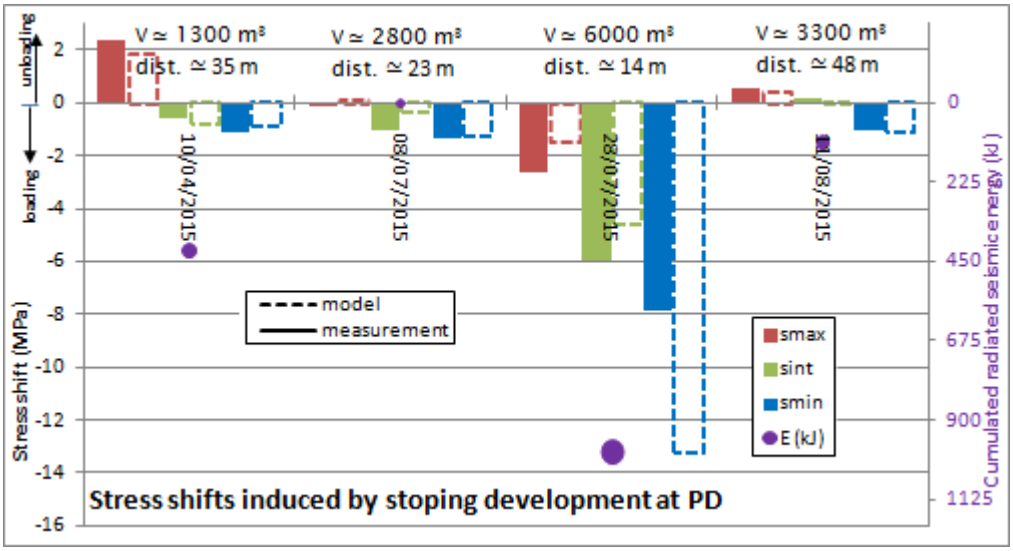

Figure 6 **Measured and modeled stress shifts (smax = major, sint = intermediary, smin = minor) induced by stoping development at PD between April and August 2015. Information on the excavated volume (V), the distance from the cells (dist.) and the cumulated radiated seismic energy (purple circle) are added.**

As a conclusion, besides all possible refinements, from the determination of the initial stress state and the

following readjustments with the recorded strain shifts, it is shown that a 3D model can most likely be calibrated on permanent stress monitoring data. Such continuous update enables to study the impact of different mining scenarios on a local area of high interest. A second potential perspective is also the computation of stress paths into a database to allow a comparison between field and predicted values on a routine basis to potentially issue an alert. This requires high-quality mine data flow in the space-time domain to remove significant artefacts in numerical modeling.

5.3 Modeling perspectives

Table 4 lists the various numerical indexes suitable for modeling continuous media. Some of those indexes are classified in rock burst categories (proneness from none to strong rockburst, Zhou et al. 2012). The main future development of this numerical model will consist, besides the mining induced stress field, in computing the most appropriate criterion for mapping seismic hazard proneness.

Table 4 Criteria and indexes of rock burst proneness computable in a numerical model.

Reference	Index	Equations
Tao (1988)	Activity index	σ_1/σ_c
Turchaninov et al. (1972)	Turchaninov criterion	$(\sigma_\theta + \sigma_1)/\sigma_c$
Barton (Tang, 2000)	-	σ_t/σ_3
Hoek & Brown (1997), Wang et al. (1998)	Criterion of tangential stress	σ_θ/σ_c
Jiang et al. (2010)	Local energy release rate	LERR = $W_e$max-$W_e$min
Wiles (2002)	Loading System Stiffness	LSS=p/ε_v
Cook (1966), Stacey & Page (1986)	Energy release rate	ERR = (W_k+W_f)/Volume
Tadjus et al. (1997)	Coefficient of energy concentration	$\beta = W_e/W_e^i$
Tadjus et al. (1997)	Coefficient of vertical stress concentration	$\sigma_{zz}/\sigma_{zz}^0$

6 Merging analysis

Stress CSIRO HI cells recorded an immediate significant stress shift on 10/04/2015 with successive time-differed stress shifts during several days that were associated with microseismicity over a whole month, while the following production of 08/07/2015, although much larger, revealed a smaller stress shift with nearly no seismicity. These observations were investigated and confirmed by the results from the modeling of a large weakness zone. Indeed, weakness zones (such as talc levels) do affect wider areas by diffusing a slower kinetic plasticity. As a consequence, the influence area of the excavated volumes is larger. This induces ductile behavior inside the weakness zones and fracturing in the nearby hard rocks (i.e. seismicity) for the stress regime to stabilize over several weeks. In this way, once next stope section is excavated, no significant seismicity or stress shift are observed since the stope has already progressively been distressed.

This behavior was observed for the important stress shift of 11/08/2015 too where seismicity was detected in the same area over 2 weeks; and more recently after first stope production at level 1182 on 26/02/2016, also located close to the weakness area. Such observations enable to confirm the progressive propagation of the stresses inside the ore, for sections containing weakness areas or not, with possible consequences of the stress transfer from the primary to the secondary stopes.

Finally, additional analysis, e.g. stress inversion calculations and accurate modeling based on mine production dataflow (geology, approximate produced ore dimensions…), possibly on new strain-shift-inducing production blasts, followed by microseismicity or not, are required to propose a longer-term valuable interpretation of such behavior.

7 Conclusion

An innovative global monitoring strategy is currently being implemented in the deeper levels of the Garpenberg mine (Lappberget orebody), where sublevel stoping method generates complex mining-induced stress fields. Induced stress fields might represent an issue to select the best mining sequence versus ground failure and seismic hazard assessment. In this monitoring, technological and geological mine data flow are being considered on a routine basis as a primary source of information to quantify and analyze the mining-induced stress state and the seismic activity. Coupling field stress and seismic monitoring along with stress prediction from 3D modeling is also part of this four-fold monitoring strategy.

During the first year of monitoring, stress changes associated with seismicity in the monitored rock mass have shown preliminary results of promising interest. First is that mining-induced seismicity and stress change rates in the surrounding rock of the freshly excavated volume appear to be closely related. Especially, important relaxation of the surrounding rock is observed when the excavation is in the limits of a large ductile area. This is most likely induced by time-dependent deformation and asymmetric stress transfer onto the hard rock medium. In this case microseismic response is staggered.

3D numerical modeling of the complete orebody including past mining levels has been calibrated based on mining-influenced stress field measurements. Initial stress field have been retrieved thanks to a computing inversion procedure that offers an excellent way to consider the stress field measurements even if acquired in an area already disturbed by the production.

Refining the geology in the model significantly reduces the discrepancy between stress change measurements and prediction, recalling here the weight of an oversimplification of the geology in mine-scale numerical simulations. This result underlines the mechanism of a time-dependent stress field arching preferentially on the hard rock medium, a phenomenon suspected of favoring dynamic instabilities and already encountered from the past experience in the mine. Shortcomings in the 3D numerical simulations could be overcame by implementing additional stress cells and geomechanical sensors in areas expected to be exploited and likely to be under the influence of weakness area.

As a further development to refine the 3D model, the choice of the most adapted criterion (numerical index) for assessing the rock burst proneness should be based on the correlation with seismic events.

Acknowledgement

This paper was written as a conclusion to INERIS-Boliden collaboration within I2Mine FP7 European Union project. The authors gratefully thank INERIS and Boliden technical staff for their invaluable support on the field and their assistance for data management on the net.

References

Abdul-Wahed, M K, Senfaute, G & Piguet, J P, 2001, 'Source location estimation using single station three-component seismic date', International symposium of the international society for rock mechanics (EUROCK 2001), June 2001, Espoo, Finland.

Amadei, B & Stephansson, O, 1997, 'Rock stress and its measurement, *Chapman & Hall*, 490 pp.

Contrucci, I, Klein, I, Bigarré, P, Lizeur, A, Lomax, A & Bennani, M, 2010, 'Management of Post-mining Large-scale Ground Failures: Blast Swarms Field Experiment for Calibration of Permanent Microseismic Early-warning Systems', *Pure Applied Geophysics*, vol. 167, pp. 43-62.

Cook, N G W, Hoek, E, Pretorius, J P G, Ortlepp, W D & Salamon, M D G, 1966, 'Rock mechanics applied to the study of rockbursts', Journal of the South African Institute of Mining and Metallurgy, vol. 66, no. 3, pp. 435–528.

Durrheim, R J, Anderson, R L, Cichowicz, A, Ebrahim-Trollope, R, Hubert, G, Kijko, A, McGarr, A, Ortlepp, W D & van der Merwe, N, 2006, 'The Risks to Miners, Mines, and the Public posed by Large Seismic Events in the Gold Mining Districts of South Africa', *Proceedings of the Third International Seminar on Deep and High Stress Mining*, 2-4 October 2006, Quebec City, Canada, J. Hadjigeorgius and M. Grenon (editors), Université Laval, Canada.

Durrheim, R J, 2010 'Mitigating the risk of Rockbursts in the deep hard rock mines in South Africa: 100 years of research. Extracting the Science: a century of mining research', *J. Brune (editor), Society for Mining, Metallurgy, and Explorations, Inc.*, ISBN 978-0-87335-322-9, pp. 156-171.

Froehlich, T, 2014, 'Guideline for geotechnical risk assessment: Geotechnical risk assessment in the Garpenberg mine, Sweden, Helsinki', Unpublished

Gibowicz, S. & Kiko,A., 1994, 'An introduction to mining seismology', *San Diego, Academic Press*.

Hoek, E & Brown, E T, 1997, 'Practical estimates of rock mass strength', *International Journal of Rock Mechanics and Mining Sciences*, vol. 34, pp. 1165-1186.

Hoek, E, 1998, 'Reliability of Hoek-Brown Estimates of Rock Mass Properties and their Impact on Design', *Int. J. Rock. Mech. Min. Sci.*, vol. 35, No. 1, pp. 63-68.

Hudyma, M R & Potvin, Y, 2004, 'Seismic hazard in Western Australian mines', *The Journal of the South African Institute of Mining and Metallurgy*, June 2004, pp. 265-276.

Hudyma, M, Potvin Y H, 2010, 'An Engineering Approach to Seismic Risk Management in Hardrock Mines', *Rock Mech. Rock Eng.*, vol. 43, pp. 891-906.

Itasca, 2012, FLAC3D (Fast Lagrangian Analysis of Continua in Three Dimensions) version 5.0, User's Guide and Command Reference. Itasca Consulting Group Inc. Minneapolis, USA.

Janiszewski, M, 2014, 'Geotechnical risk assessment in the Pyhäsalmi mine with a focus on seismic risk', Master Thesis, Aalto University.

Jiang, Q, Feng, X T, Xiang, T B & Su, G.S., 2010, 'Rockburst characteristics and numerical simulation based on a new energy index: a case study of a tunnel at 2500 m depth', *Bulletin of Engineering Geology and the Environment*, vol. 69, pp. 381-388.

Lahaie, F, Gunzburger, Y, Ben Ouanas, A, Barnichon, J D, Bigarré, P & Piquet, J P, 2010, 'Impact of epoxy glue curing time on the quality of overcoring stress measurements in low-temperature environments', *Rock Stress and Earthquakes – Xie (ed), London*, pp. 161-166.

Larsson, K, 2004, 'Mining Induced Seismicity in Sweden', Licentiate Thesis, Luleå University of Technology.

Levenberg, K, 1944, 'A Method for the Solution of Certain Problems in Least Squares', *Quart. Appl. Math.*, Vol. 2, pp. 164-168.

Lizurek, L, Rudziński, L & Plesiewicz, B, 2014, 'Mining induced seismic event on an inactive fault', *Acta Geophysica*, pp 1-25.

Lomax, A, Virieux, J, Volant, P & Berge, C, 2000, 'Probabilistic earthquake location in 3D and layered models: Introduction of a Metropolis-Gibbs method and comparison with linear locations', *Advances in Seismic Event Location*, Thurber, C.H., and N. Rabinowitz (eds.), Kluwer, Amsterdam, pp. 101-134.

Magrota, N, Ahmed, N & Chael, E, 1987, 'Seismic event detection and source location using single-station (three component) data', *BSSA*, vol. 77 (3), pp. 958-971.

Maleki, H N, 1990, 'Development of modelling procedures for coal mine stability evaluation', *Proc. 31st US Symposium of Rock Mechanics*, Golden, Balkema, Rotterdam, pp. 85-92.

Matrullo, E., Lizeur, A., Contrucci, I., Tonnellier, A. & Bigarré, P., 2015, 'Practical guide to assess seismic array performance', *INERIS internal document, DRS-15-127366-06061B*.

Nyström, A, 2003, ‚Bergmekaniska observationer och arbeten I G9 03v47', Internal report Boliden Mineral AB (in Swedish).

Ortlepp, W D, 1997, 'RaSiM Comes of Age—A Review of the Contribution to the Understanding and Control of Mine Rockbursts SRK Consulting', Johannesburg, 1997

Pasquet, S, 2014, 'Apport des méthodes sismiques à l'hydrogéophysique: importance du rapport Vp/Vs et contribution des ondes de surface', PhD Thesis, UPMC.

Potvin, Y & Wesseloo, J, 2013, 'Improving seismic risk management in hardrock mines', *Eighth International Symposium on Rockbursts and Seismicity in Hardrock Mines, vol. 1, Geophysical Survey of Russian Academy of Sciences, Russia, pp. 371-386.*

Szczerbowski, Z & Jura, J, 2015, 'Mining induced seismic events and surface deformations monitored by GPS permanent stations', *Acta Geodyn. Geomater.*, vol. 12, No. 3 (179), pp. 237–248.

Stacey, T R & Page, C H, 1986, 'Practical Handbook for Underground Rock Mechanics', *Trans-Tech. Publ.*

Tajdus, A, Flisiak, J & Cala M., 1997, 'Estimation of rockburst hazard basing on 3D stress field analysis', *Rockbursts and Seismicity in Mines*, Gibowicz & Lasocki (ed.), Balkema, Rotterdam, ISBN 9054 108908, pp. 272-277.

Tang, B Y , 2000, 'Rockburst Control using Distress Blasting', Ph.D. Dissertation. McGill University, Montreal, Canada.

Tao, Z Y, 1988, 'Support design of tunnels subjected to rockbursting', *Romana (Ed.), ISRM International Symposium, Rock Mechanics and Power Plants*, pp. 407–411.

Turchaninov, I A, Markov, G A, Gzovsky, M V, Kazikayev, D M, Frenze, U K, Batugin, S A & Chabdarova, U I, 1972, 'State of stress in the upper part of the Earth's crust based on direct measurements in mines and on tectonophysical and seismological studies', *Physics of the Earth and Planetary Interiors*, vol. 6, pp. 229-234.

Volker, O & Roth, M, 2003, 'Automated seismic event location for hydrocarbon reservoir', *Computer and Geosciences*, vol. 29, pp. 851-863.

Wang, Y H, Li, W D, Li, Q G, Xu, Y & Tan, G H, 1998, 'Method of fuzzy comprehensive evaluations for rockburst prediction', *Chinese Journal of Rock Mechanics and Engineering*, vol. 17, No. 5, pp. 493–501 (in Chinese).

Wiles, T D, Marisett, S D & Martin, C D, 1998, 'Correlation Between Local Energy Release Density and Observed Bursting Conditions at Creighton Mine', *Mine Modelling Report*, Sudbury, Canada.

Wiles, T D, 2002, 'Loading system stiffness - A parameter to evaluate rockburst potential', *1st Int. Seminar on Deep and High Stress Mining*, Perth, Australia.

Zhou, J, Li, X & Shi, X, 2012, 'Long-term prediction model of rockburst in underground openings using heuristic algorithms and support vector machines', *Safety Science*, vol. 50, pp. 629-644.

Zinszner, B & Pellerin, F M, 2007, 'A geoscientist's guide to geophysics', *Editions Technip*.